Water Splitting on Titanium Oxide nanomaterial: a theoretical investigation

Lila Ballav Pandey
Oxford College, Shanti Secondary School, Tilottama, Nepal
lbpandeyka@gmail.com
Received: Aug 20, Reviewed: 11 Oct, Revised: 20 Oct, Accepted: Dec 19

Abstract

The step-by-step electrochemical mechanism of water splitting by removal of protons and electrons is examined for the reaction of one and two water molecules on a Ti_2O_4 cluster. Density functional theory (B3LYP) and coupled cluster single-point calculations are employed to compute gas-phase reaction energies. The Polarizable Continuum Model (PCM) is utilized to calculate energies in the aqueous phase. Both neutral and alkaline media are considered. Proton and electron removal steps are generally found to be highly endothermic, except for proton removal steps in alkaline medium. The effect of an external potential on reaction energies is considered. Oxygen-oxygen bonds form after the removal of only two electrons (or one electron for the one water case).

Keywords: Electrochemical mechanism, sustainable energy, heterogeneous catalyst, polarizable continuum model.

Introduction

Water splitting over photoexcited semiconductor photocatalysts to yield hydrogen and oxygen has been recognized as an alternative and one of the most sustainable energy sources for the next generation. Extensive studies on photocatalytic water splitting on semiconductor oxide surfaces have been performed since the pioneering work of Fujishima and Honda (1972) on this reaction over titanium oxide. Absorption of UV radiation of ~400 nm is required to dissociate water (Fujishima & Honda, 1972; Anpo et al., 2006). One difficulty in this dissociation is the high overpotential needed at the photoanode, so numerous studies have looked at ways to reduce this, including doping of TiO_2 to reduce its band gap (Asahi et al., 2001; Di Valentin et al., 2005; Karvinen et al., 2003; Xu et al., 2007; Shankar et al., 2006).

Titanium oxide is an important catalyst as it is abundant, non-toxic, and stable. This oxide has been studied extensively in water splitting reactions as a heterogeneous catalyst. Since the photochemical reaction mechanism may be expected to be similar in many respects to the electrochemical pathway involving proton and electron removal from water, studies of the electrochemical mechanism could yield insights in both areas. Electrochemical step-by-step hydrogen transfer requires an additional electrical potential. Previous theoretical work by Valdés et al. (2008) accounted for the overpotential for hydrogen removal on titanium dioxide slabs at different pH. At 0 V, the reaction path was predicted to be uphill for the loss of all hydrogens of the reaction $2H_2O \rightarrow 4H + O_2$. They found that the overall reaction will be downhill at and above 2.20 V. The external potential for such hydrogen loss falls significantly (by 0.83 V) at higher pH, so alkaline media aids the reaction. The first step was found to be the rate-limiting step. In addition, oxygen–oxygen bonds form

(as a hydroperoxy intermediate) after the release of three hydrogens (Valdés et al., 2008). In related work, overpotentials have been determined for the water splitting reaction on RuO_2, IrO_2, and TiO_2 surfaces (Rossmeisl et al., 2007). Recent work by Li et al. (2010) suggests that the first proton removal step dictates the high overpotential on TiO_2.

The reverse reaction of oxygen reduction into water and hydrogen oxidation into water on platinum surfaces is of interest for use in fuel cells (Hyman & Medlin, 2005, 2006). Previous theoretical work has shown that a chain of water molecules mediates proton transfer and connects the oxygen reduction reaction at coordinately unsaturated active sites (Hyman & Medlin, 2005, 2006). The suggested mechanism has a hydroperoxy intermediate in the initial step of oxygen reduction (Hyman & Medlin, 2005, 2006).

Although most theoretical work on TiO_2 has focused on extended surfaces (Valdés et al., 2008; Li et al., 2010; Hussain et al., 2010; Lindan & Zhang, 2005), some recent work has also examined water splitting reactions on TiO_2 nanotubes (Meng et al., 2011) or large clusters (Valdés & Kroes, 2010) and hydrolysis reactions on small $(TiO_2)_n$ (n = 1–4) clusters (Wang et al., 2011).

In this work, we focus on the water splitting reaction on a small Ti_2O_4 cluster. The structure of Ti_2O_4 has previously been determined to have C_2h symmetry (Hagfeldt et al., 1993; Jeong et al., 2000; Qu & Kroes, 2006; Calatayud et al., 2008; Li & Dixon, 2008; Zhai & Wang, 2007; Bandyopadhyay & Aikens, 2011). Cluster models have the advantage that the electron and proton loss processes can be examined separately, since charge neutrality does not need to be maintained unlike systems involving periodic boundary conditions. In order to study water splitting reactions, the ease of proton loss must be calculated. Reaction energies for $HA + OH^- \rightarrow A^- + H_2O$ and pKa values for proton loss from acids HA can be calculated by established literature procedures (Pliego & Riveros, 2001, 2002) using models such as the polarizable continuum model (PCM) (Tunon et al., 1992).

Despite a number of theoretical investigations of the water oxidation reaction, the actual mechanism of water oxidation is still unknown in both neutral and alkaline media. This study probes the electron and the proton loss mechanisms on the molecular level so that they can be generalized to the bulk level on the basis of different water-coordinated titanium molecules in gas phase as well as in alkaline aqueous phase. Furthermore, we suggest intermediate structures for the explanation of the initiation of oxygen–oxygen bond formation. Triplet states are considered, although the triplet state pathway is still found to be high-energy. This article also investigates the use of an applied electrical potential to make the reaction steps more feasible.

Methods and Procedure

The general atomic and molecular electronic structure system (GAMESS) (Schmidt et al., 1993) software has been used for all calculations in this work. The Ti_2O_4 molecule, other structures made by adding one and two water molecules, and intermediate structures involving proton and electron loss have been optimized with the B3LYP/TZV(d, p) level of theory. For systems with an even number of electrons, singlet and triplet spin states have been examined; doublet states are

considered for odd number of electrons. A restricted open-shell formalism is used for doublet and triplet states. Coupled cluster singles and doubles (CCSD) single point energies are also calculated at the optimized intermediate structures in the titanium oxide water splitting mechanism. The water splitting reaction energy is calculated by CCSD with basis sets up to the pentuple zeta level. Hessian calculations are performed to determine the zero-point energy (ZPE) as well as thermodynamic quantities like entropy, specific heat capacity, and enthalpy corrections needed to calculate free energies of the reaction at 298K.

By incorporating a continuum dielectric solvent using the polarizable continuum model (PCM) and re-optimizing structures, energies are calculated in aqueous phase. The cavity is based on Van der Waals (VDW) radii as specified in GAMESS. Calculations of pKa's have been carried out using the PCM model and established literature procedures (Pliego & Riveros, 2001, 2002). The electronic energy of $HA + H_2O \rightarrow A^- + H_3O^+$ is corrected by adding zero point energy. In this solvent model, the energy contribution by entropy has been neglected and the solvation free energy is calculated by the formula $\Delta G^*_{sol} = \Delta G^*_{gas} + \sum\left[\Delta G^*_{product} - \Delta G^*_{react}\right]$. The free energy change in gaseous state (ΔG^*_{gas}) is added with difference in free energy of the reaction ($\Delta G^*_{product} - \Delta G^*_{react}$) in solution phase. This calculated free energy of solvation is included to calculate the pKa value of the proton loss step by the well-known relation:

$$\Delta G = -RT\ln K$$

Reaction energies of proton loss reactions are also calculated for the reaction in alkaline medium:

$$HA + OH^- \rightarrow A^- + H_2O$$

Results and Discussion

Uncatalyzed Water Splitting Reactions

The reaction energy of $H_2O \rightarrow H_2 + ½\ O_2$ has been calculated at different levels of theory. Water, hydrogen, and oxygen molecules have been optimized at the B3LYP/TZV(d, p) level, and the reaction energy is found to be 57.92 kcal/mol at 0K. In order to determine the free energy change of the reaction, the following procedure is employed. First, Hessian calculations are performed to get the zero-point energy (ZPE). The enthalpy change at 0K is computed by $\Delta H^{0K} = \Delta E(B3LYP) + \Delta ZPE$ to be 52.16 kcal/mol. The enthalpy change at 298K is calculated by taking into consideration the variation in specific heat capacity with temperature:

$$\Delta H^{298K} = \sum_{\text{reactant}}\left(\mathrm{H}(298) - H(0)\right) + \Delta H^{0K} + \sum_{product}\left(H(0) - H(298)\right)$$

Enthalpy corrections and entropies at 298K (Table 1) are also obtained from Hessian calculations; including the enthalpy correction, the reaction energy decreases to 51.09 kcal/mol.

Table 1

B3LYP/TZV(d, p) Thermodynamic Quantities of Water, Hydrogen, and Oxygen.

Quantities\Species	Enthalpy Correction H(T)-H(0) (kcal/mol)	Entropy (S) (cal/mol-K)
Water	2.074	45.076
H_2	0	31.136
O_2	2.004	48.986

The free energy of reaction at 298K is calculated by $\Delta G^{298K} = \Delta H^{298K} - T\Delta S$ to be 50.79 kcal/mol. The calculated B3LYP/TZV(d, p) reaction energy underestimates the experimental value (1.23 eV, 56.75 kcal/mol) by about 6 kcal/mol. To check the convergence of the reaction energy with better methods and basis sets, the reaction energies are also calculated with CCSD single point calculations using basis sets from cc-pVDZ to cc-pV5Z. Table 2 lists the energy of the reaction and free energy change with variation in level of theory. If one assumes that coupled cluster calculations primarily affect the electronic energy of the reaction and not the ZPE or thermodynamic quantities, we can improve the B3LYP/TZV(d,p) values by adding a correction for the method/basis set. The calculated energy generally increases with the quality of basis set. There is significant improvement in energy (~3 kcal/mol) from double zeta level to triple zeta level. The reaction energy is predicted to be 0.3-0.4 kcal/mol higher with the TZV(d, p) basis set compared to the cc-pVTZ basis set. Increasing the basis set to cc-pV5Z leads to a ΔG^{298} value of 55.35 kcal/mol, in good agreement with experiment. Although a small improvement in energy from triple zeta level to higher basis sets is noted, triple zeta basis sets will be used in the remainder of this work because they represent a good balance of accuracy and efficiency. Overall, the reaction energy improved with the coupled cluster method compared to B3LYP by almost 4 kcal/mol with the TZV(d, p) basis set; thus, coupled cluster single point calculations will be employed in this work to improve the B3LYP reaction energies.

Table 2

Reaction Energies (kcal/mol) for $H_2O \longrightarrow H_2 + \frac{1}{2}O_2$ *with Different Levels of Theory*

Level of Theory	ΔE^{0K}	ΔH^{298K}	ΔG^{298K}
B3LYP/TZV(d, p)	57.97	53.94	50.79
B3LYP/cc-pVTZ	57.65	53.61	50.47
CCSD/cc-pVDZ	54.21	54.36	51.22
CCSD/TZV(d, p)	57.97	57.73	54.58
CCSD/cc-pVTZ	60.95	57.26	54.12
CCSD/cc-pVQZ	63.32	58.13	54.99

Level of Theory	ΔE^{0K}	ΔH^{298K}	ΔG^{298K}
CCSD/cc-pV5Z	63.89	58.49	55.35
Experimental			56.75

In addition to the reaction above, the half-reaction $H_2O \rightarrow 2H^+ + 2e^- + ½\ O_2$, yielding protons and electrons, is also considered. At the B3LYP/TZV(d, p) level of theory, the reaction energy in gas phase is calculated to be 794.06 kcal/mol. In addition, the single point energy at the CCSD/TZV(d, p) level is determined to be 796.68 kcal/mol, which means that the coupled cluster calculations differ from B3LYP calculation by only 2.62 kcal/mol (0.3%). In the aqueous phase, the reaction energy is significantly reduced to 594.02 kcal/mol at the PCM-B3LYP/TZV(d, p) level of theory, so solvent effects are important to consider in the water splitting process.

Catalyzed water splitting reactions

The first step in the examination of the electrochemical water splitting mechanism involves the reaction of a water molecule with titanium oxide dimer. The binding energy of the water molecule is predicted to be 21.0 kcal/mol at the B3LYP/TZV(d, p) level of theory. This binding energy is in good agreement with experimental physisorption energies of 14-24 kcal/mol,[29-31] although it should be noted that experimental values are measured for a bulk surface whereas these calculations are performed on a cluster. Our calculated values are in good agreement with the most recent theoretical results for H_2O adsorption on Ti_2O_4, which predict a physisorption energy of 29.5 kcal/mol at the B3LYP/DZVP2 level of theory (Wang et al., 2011). Two transition state geometries are optimized in this work: the water molecule can dissociate so that the hydroxyl group bonds with a titanium atom and the proton goes either to a terminal oxygen or to a bridging oxygen atom (Figure 1). Although the transition states are 12.8 and 15.5 kcal/mol higher, respectively, than the intermediate state of the addition product, they have lower energy than the reactants. Thus, the reaction can proceed directly to products. In either reaction pathway, the O-H bond dissociation process is exothermic by 60.2-60.4 kcal/mol. This is in good agreement with recent theoretical results that predict a dissociation energy of 57.7 kcal/mol for the first water molecule (Wang et al., 2011).

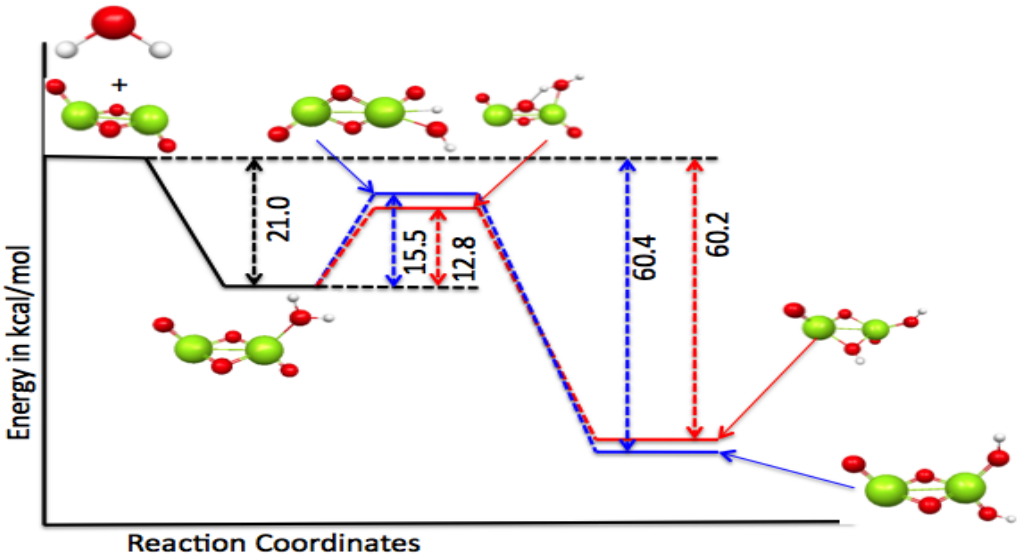

Figure 1: Reaction Pathway Showing the Formation of Addition Product Between Ti_2O_4 and two Water Molecules.

To probe the electrochemical mechanism of the reaction on the titanium oxide cluster, proton loss and electron loss steps are studied. Structures of the anions formed by proton-dficient intermediates and cations formed by releasing electrons are optimized with the same level of theory.

One water molecule

$Ti_2O_5H_2$ may undergo electron loss to form the $Ti_2O_5H_2^+$ cation or several proton loss possibilities to form $Ti_2O_5H^-$. Both steps are endothermic, with reaction energies shown in Figure 2. Proton loss from $Ti_2O_5H_2^+$ and electron loss from $Ti_2O_5H^-$ produce neutral Ti_2O_5H. The release of another proton from $Ti_2O_5H^-$ to form the divalent anion $Ti_2O_5^{2-}$ is found to be highly endothermic. Proton loss from neutral Ti_2O_5H structures and electron loss from $Ti_2O_5^{2-}$ can produce the $Ti_2O_5^-$ anion. Proton loss steps are more than 300 kcal/mol endothermic, whereas the electron loss step is exothermic by -20 kcal/mol for this case. One more pathway of electron loss with a reaction energy of ~200 kcal/mol has also been studied with Ti_2O_5H structures to get $Ti_2O_5H^+$. In the optimized $Ti_2O_5H^+$ (a) and (b) structures, a μ-O_2 structure is formed either bridging the titanium atoms (a) or at the terminal position (b). Proton loss from $Ti_2O_5H^+$ as well as electron loss from $Ti_2O_5^-$ results in Ti_2O_5 with one oxygen-oxygen bridging bond. The reaction energy to release oxygen from Ti_2O_5 is calculated to be 150.2 kcal/mol at the B3LYP/TZV(d, p) level of theory (Figure 2). It should be noted that the oxygen molecule is a triplet in its most stable state. Triplet states have been examined for systems that have lost two electrons, but these are higher in energy than the corresponding singlet states.

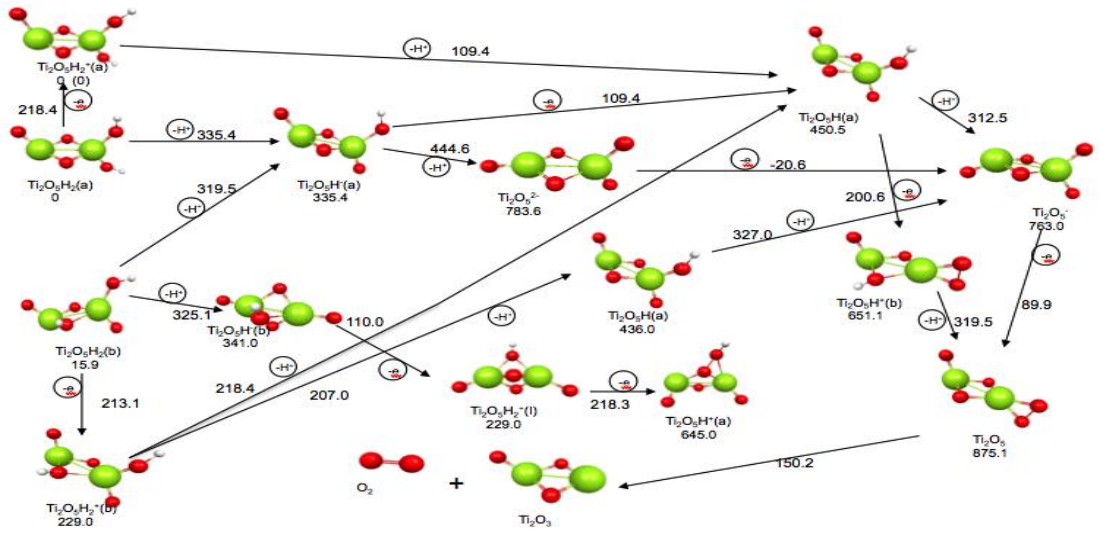

Figure 2: Reaction Flow Chart of Proton and Electron Loss from one Water Molecule with Ti_2O_4

Full reaction energies are shown in Tables 3 and 4. PCM stabilizes singly charged species by ~40-50 kcal/mol relative to gas phase calculations, whereas neutral species are essentially not affected (energies typically change by < 3 kcal/mol). Doubly charged $Ti_2O_5^{2-}$ is stabilized by ~160 kcal/mol.

Two water molecules

Five different geometries of the addition product of Ti_2O_4 with two water molecules have been optimized, and the energy of the reaction has been calculated (Figure 3). Structures are abbreviated by alphabetical letters (a, b, c …) in increasing order of the energies of corresponding structures. All energies are found to be negative, as in the one water molecule case. Structure (a) has the lowest energy; structure (b) is similar. Due to an inability to optimize the electron loss step for these two systems, structure (c) has been chosen as the structure from which proton loss and electron loss processes are studied in the most detail.

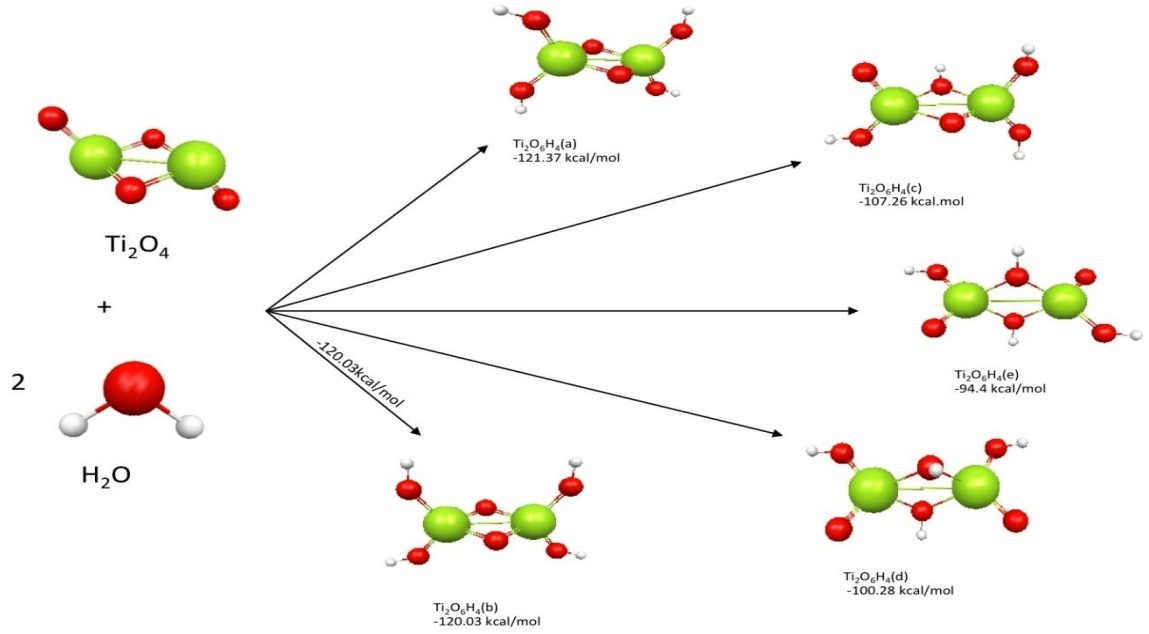

Figure 3: Formation of Intermediates of Ti_2O_4 with two Water Molecules

Three different geometries have been optimized for proton loss, and one electron loss structure has been optimized from the $Ti_2O_6H_4$ structure (c) (Figure 4). Proton loss is calculated to be highly endothermic by more than 300 kcal/mol. Formation of a cation by losing an electron is endothermic by 213.3 kcal/mol. Two structures for the electron loss step have been optimized from $Ti_2O_6H_3^-$ anions (a) and (c) with reaction energies of 81.0 and 105.6 kcal/mol. The electron loss structure from $Ti_2O_6H_3^-$(b) did not optimize.

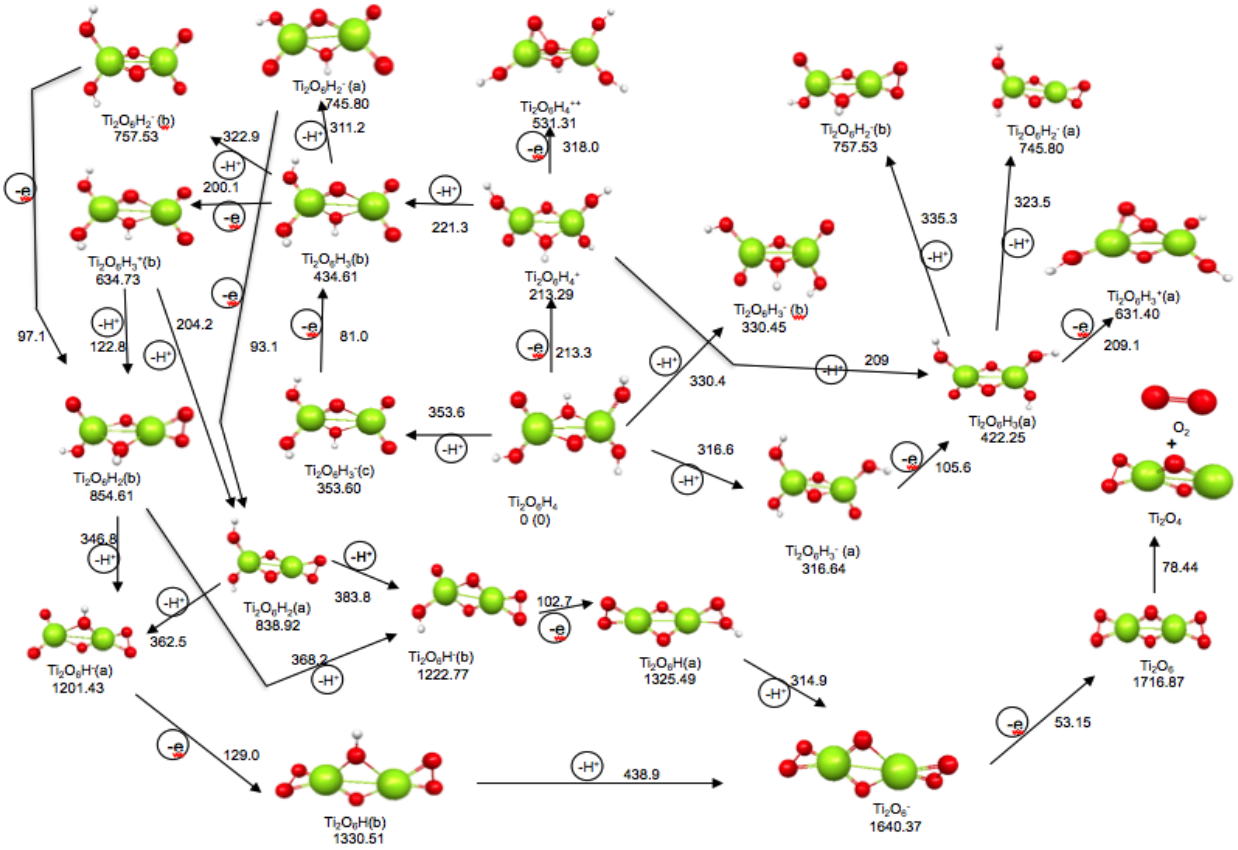

Figure 4: Reaction Flow Chart of Proton and Electron Loss From two Water Molecules with Ti_2O_4 (Energies In Kcal/Mol)

Further optimization of geometries for the removal of extra electrons and protons was carried out with $Ti_2O_6H_3$ geometries. Electron loss steps to yield two $Ti_2O_6H_3^+$ structures require absorption of 122 or 204 kcal/mol energy. Proton loss steps leading to the formation of $Ti_2O_6H_2^-$ were found to be endothermic by more than 300 kcal/mol. Removal of an electron from $Ti_2O_6H_2^-$ created an oxygen-oxygen bond at the terminal position; terminal O-O Bonds are also formed when protons are removed from $Ti_2O_6H_3^+$. Similarly, a bridging O-O A bond was also created by electron removal from $Ti_2O_6H_4^+$ to yield $Ti_2O_6H_4^{2+}$. A third proton loss step was carried out from $Ti_2O_6H_2$ to get $Ti_2O_6H^-$ geometries. The reaction energies in this process are higher than those for the removal of the first proton from $Ti_2O_6H_4$ to get $Ti_2O_6H_3$ and for the second proton from $Ti_2O_6H_3$ to $Ti_2O_6H_2$. Both (a) and (b) optimized geometries of $Ti_2O_6H^-$ sustained the oxygen-oxygen bridge upon removal of the third proton. Continuing on this process, two geometries of Ti_2O_6H are optimized by taking off the third

electron although these processes require more than 100 kcal/mol. In a similar fashion, the last proton from Ti_2O_6H was abstracted to make the $Ti_2O_6^-$ intermediate. The reaction energy for Ti_2O_6H(a) is 314.9 kcal/mol, whereas for Ti_2O_6H(b) it is 438.9 kcal/mol. Finally, the last electron was removed from $Ti_2O_6^-$ which required 53.2 kcal/mol to make the Ti_2O_6 molecule in a singlet state. The triplet state of the molecule was also optimized, but it has a higher energy than the singlet state geometry. The reaction energy to break Ti_2O_6 into Ti_2O_4 and triplet O_2 was calculated to be 78.4 kcal/mol. It should be noted that the structure of the catalyst significantly changed from its original geometry. The difference in energy between the final and initial Ti_2O_4 structures is calculated to be 99.9 kcal/mol (Figure 5).

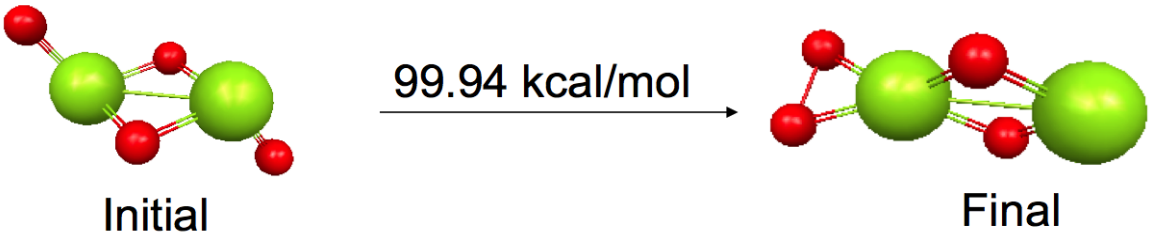

Figure 5: Change in Geometry of Ti_2O_4 Catalyst During Proton and Electron loss Process

Formation of O-O bonds

As the goal of the project demands, the formation of O_2 at the anode is of high interest. Probes on initiation of oxygen-oxygen bond formation have been carried out systematically; O-O bond formation is observed after losing only two electrons. One of the pathways is from the $Ti_2O_6H_4$ geometry when loss of two electrons consequently makes an O-O bridge at the bridging position. Similarly, $Ti_2O_6H_2$ geometries are obtained with bridging oxygen both at the terminal position and at the bridging position. Bridging oxygen geometries are seen in both one and two-water molecule systems. In the one water molecule case, the bridging O-O species is observed even after one electron is removed. An O-O bond length of ~1.44 Å has been calculated in the bridging oxygen geometries which is longer than the O=O double bond (1.21 Å) in the O_2 molecule and is similar to the bond in peroxide (1.48 Å). In addition, unscaled harmonic vibrational frequencies are calculated for the O-O species: these values are computed to be ~870-890 cm^{-1} in the bridging (B) position and ~920-940 cm^{-1} in the terminal (T) position (Figure 6).

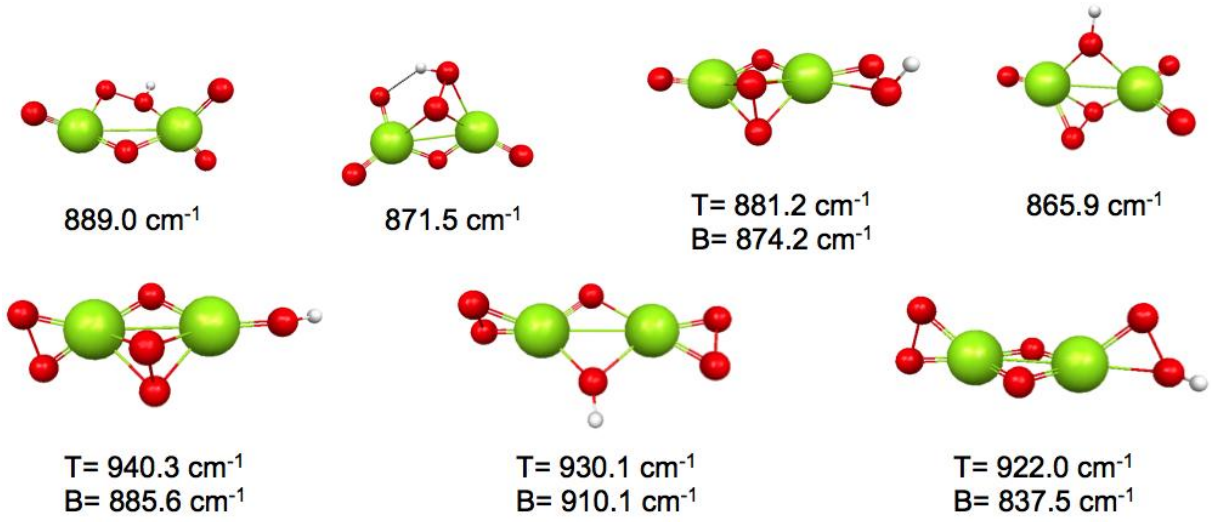

Figure 6: Stretching Frequencies of Oxygen-Oxygen Bonds Formed in Ti_2O_6H Structures

Experimental work by Nakamura and Nakato (2004, 2005) suggested that TiOOH and TiOOTi species are produced as primary intermediates in water splitting, with vibrational bands at 838 and 812 cm^{-1}. Several previous theoretical studies have considered hydroperoxy intermediates (Valdés et al., 2008; Hyman & Medlin, 2005, 2006), although this has been questioned recently (Li et al., 2010). In our work, all of the HOO-containing structures lie at higher energy than isomers with the same stoichiometry that do not contain the hydroperoxy moiety. This work suggests that pathways that do not involve the hydroperoxy species should be considered in addition to those involving HOO species as a primary intermediate.

PCM calculations

Single-point energies are calculated, including solvent, by the PCM model. These energies are found to be comparable to and lower than those for the gas phase reaction. Solvation energies for all species are listed in Table 3. Solvation energies for neutral complexes range from -9 to -19 kcal/mol, while solvation energies for singly charged titanium-containing species range from -50 to -66 kcal/mol. Solvation energies for doubly charged systems are much higher, and range from -177 to -191 kcal/mol.

Table 3

PCM-B3LYP/TZV (d, p) Solvation Energies (kcal/mol) of Reaction Intermediates

H^+	-113.81	Ti_2O_5(3)	22.62	$Ti_2O_6H_2^-$(c)	-0.01
OH^-	-91.10	$Ti_2O_6H_4$(a)	-11.03	$Ti_2O_6H_2$(a)	-10.55
H_2O	-6.52	$Ti_2O_6H_4$(e)	278.51	$Ti_2O_6H_2$(b)	-14.15
Ti_2O_5H(a)	-14.39	$Ti_2O_6H_4$(d)	-15.63	$Ti_2O_6H_2$(c)	-10.06
Ti_2O_5H(b)	-18.70	$Ti_2O_6H_4$(c)	-13.99	$Ti_2O_6H^-$(b)	-52.68
$Ti_2O_5H^-$(a)	-61.12	$Ti_2O_6H_4$(b)	-11.56	$Ti_2O_6H^-$(a)	-62.64
$Ti_2O_5H^-$(b)	-60.50	$Ti_2O_6H_4^+$(c)	-52.09	Ti_2O_6H(a)	-12.45
$Ti_2O_5H^-$(c)	-56.17	$Ti_2O_6H_4^{2+}$(c)	-178.65	Ti_2O_6H(b)	-14.03
$Ti_2O_5H^+$(a)	-56.06	$Ti_2O_6H_3^-$(b)	-57.95	Ti_2O6^{2--}	-177.08

$Ti_2O_5H^+$(3)	-56.22	$Ti_2O_6H_3^-$(a)	-56.31	$Ti_2O_6^-$	-51.00
$Ti_2O_5H^+$(b)	-62.88	$Ti_2O_6H_3^-$(c)	-66.24	Ti_2O_6	-9.32
$Ti_2O_5H_2^+$(b)	-64.53	$Ti_2O_6H_3$(c)	-15.67	Ti_2O_4 (Final)	-11.06
$Ti_2O_5H_2^+$(a)	-53.93	$Ti_2O_6H_3$(a)	-9.92	Ti_2O_4 (Initial)	-18.98
$Ti_2O_5H_2$(b)	-18.98	$Ti_2O_6H_3$(b)	-13.62	$Ti_2O_6H_2^-$(c)	-0.01
$Ti_2O_5H_2$(a)	-15.38	$Ti_2O_6H_3^+$(c)	-57.81	$Ti_2O_6H_2$(a)	-10.55
$Ti_2O_5H_2^{2+}$(a)	-190.81	$Ti_2O_6H_3^+$(a)	-49.85	$Ti_2O_6H_2$(b)	-14.15
Ti_2O_5	-15.09	$Ti_2O_6H_3^+$(b)	-55.03	$Ti_2O_6H_2$(c)	-10.06
$Ti_2O_5^-$	-58.10	$Ti_2O_6H_2^-$(a)	-53.47	$Ti_2O_6H^-$(b)	-52.68

Tables 4 and 5 list the reaction energies for proton loss and electron loss steps, respectively, in gas and aqueous phases. The free energy of the reaction is also calculated for each reaction in gas phase. Gas phase reactions are all uphill either in proton loss or in electron loss steps, but the reaction energies of the proton loss steps in alkaline medium, $HA + OH^- \longrightarrow A^- + H_2O$, are calculated to be negative in most cases (Table 6). Proton loss for cationic and neutral species is predicted to yield fairly negative ΔG values (-10 to -193 kcal/mol), but the free energy change is calculated to be positive for proton loss from anionic $Ti_2O_5H^-$. Table 4 shows the free energy of the reaction for the proton loss processes in reaction steps of $Ti_2O_6H_4$ and $Ti_2O_5H_2$. pKa's of several proton loss steps are tabulated in Table 6. These pKa values clearly explain the ease of separation of proton in the increasing order from anionic, neutral, and cationic species. Calculated values are reasonably high in case of cationic species, which makes sense because proton loss from positively charged species is relatively facile. In contrast, proton loss from an anionic system is almost impossible.

Table 4

Reaction Energies for Proton Loss Processes in Gas and Aqueous Phases.

Reactions	ΔE^{0K} B3LYP/ TZV(d,p) (kcal/mol)	ΔE^{0K} PCM-B3LYP/ TZV(d,p) (kcal/mol)	ΔE^{0K} CCSD/ TZV(d,p) (kcal/mol)	ΔH^{298K} B3LYP/ TZV(d,p) (kcal/mol)	ΔG^{298K} B3LYP/ TZV(d,p) (kcal/mol)
$Ti_2O_5H_2$(b)→$Ti_2O_5H^-$(b)	319.9	278.3	339.3	313.6	314.9
$Ti_2O_5H_2^+$(a)→Ti_2O_5H(a)	217.6	257.1	220.2	218.4	219.3
$Ti_2O_5H_2^+$(b)→Ti_2O_5H(a)	207.0	257.1	215.9	207.7	209.7
$Ti_2O_5H^-$(a)→$Ti_2O_5^{2-}$	448.3	319.4	455.1	441.2	441.1
Ti_2O_5H(a)→$Ti_2O_5^-$	327.0	283.3	331.9	320.7	321.4
Ti_2O_5H(b)→$Ti_2O_5^-$	312.5	273.1	321.5	306.6	308.1
$Ti_2O_6H_4$(c)→$Ti_2O_6H_3^-$(b)	330.4	286.5	334.4	324.4	326.4
$Ti_2O_6H_4$(c)→$Ti_2O_6H_3^-$(a)	316.6	274.3	322.9	308.7	308.1
$Ti_2O_6H_4$(c)→$Ti_2O_6H_3^-$(c)	353.6	301.4	361.4	346.8	347.2
$Ti_2O_6H_4^+$(c)→$Ti_2O_6H_3$(a)	209.0	251.1	213.0	201.2	198.4

Reactions	ΔE^{0K} B3LYP/ TZV(d,p) (kcal/mol)	ΔE^{0K} PCM-B3LYP/ TZV(d,p) (kcal/mol)	ΔE^{0K} CCSD/ TZV(d,p) (kcal/mol)	ΔH^{298K} B3LYP/ TZV(d,p) (kcal/mol)	ΔG^{298K} B3LYP/ TZV(d,p) (kcal/mol)
$Ti_2O_6H_4$+(c)→$Ti_2O_6H_3$(c)	230.2	266.6	225.0	224.6	224.9
$Ti_2O_6H_3$(b)→$Ti_2O_6H_2^-$(a)	311.2	271.3	328.1	304.5	305.5
$Ti_2O_6H_3$(b)→$Ti_2O_6H_2^-$(b)	323.7	337.4	328.1	318.0	319.5
$Ti_2O_6H_3$(b)→$Ti_2O_6H_2^-$(c)	314.9	330.5	324.6	307.8	306.4
$Ti_2O_6H_3$(a)→$Ti_2O_6H_2^-$(a)	323.5	280.0	336.5	317.7	318.9
$Ti_2O_6H_3$(a)→$Ti_2O_6H_2^-$(b)	335.3	290.0	335.4	330.5	332.2
$Ti_2O_6H_3^+$(b)→$Ti_2O_6H_2$(a)	204.4	248.8	210.3	198.4	200.0
$Ti_2O_6H_3^+$(b)→$Ti_2O_6H_2$(b)	220.1	261.0	221.6	215.3	217.3
$Ti_2O_6H_2$(a)→$Ti_2O_6H^-$(a)	362.5	310.4	366.8	356.2	356.4
$Ti_2O_6H_2$(a)→$Ti_2O_6H^-$(b)	383.9	341.7	402.2	378.7	380.6
$Ti_2O_6H_2$(b)→$Ti_2O_6H^-$(a)	346.8	298.3	355.4	339.3	339.0
$Ti_2O_6H_2$(b)→$Ti_2O_6H^-$(b)	368.1	329.6	390.8	361.8	363.2
Ti_2O_6H(a)→$Ti_2O_6^-$	314.8	276.3	319.9	306.8	306.3

Table 5

Reaction energies for electron loss processes in gas and aqueous phases

Reactions	ΔE^{0K} B3LYP/ TZV(d,p) (kcal/mol)	ΔE^{0K} PCM-B3LYP/ TZV(d,p) (kcal/mol)	ΔE^{0K} CCSD/ TZV(d,p) (kcal/mol)	ΔH^{298K} B3LYP/ TZV(d,p) (kcal/mol)	ΔG^{298K} B3LYP/ TZV(d,p) (kcal/mol)
$Ti_2O_5H_2$(a)→$Ti_2O_5H_2^+$(a)	218.4	179.9	214.2	217.9	179.1
$Ti_2O_5H_2$(b)→$Ti_2O_5H_2^+$(b)	213.1	167.6	218.6	213.2	213.3
$Ti_2O_5H^-$(a)→Ti_2O_5H(a)	100.6	147.4	95.0	100.2	99.5
$Ti_2O_5H^-$(b)→Ti_2O_5H(b)	114.7	156.5	105.7	113.8	112.5
Ti_2O_5H(a)→$Ti_2O_5H^+$(b)	215.1	166.6	208.7	216.5	217.3
Ti_2O_5H(b)→$Ti_2O_5H^+$(a)	194.5	157.2	191.4	195.4	196.6
$Ti_2O_5^{2-}$→$Ti_2O_5^-$	-20.6	111.2	-28.2	-20.3	-20.2
$Ti_2O_5^-$→Ti_2O_5	89.9	132.9	88.9	91.2	92.3
$Ti_2O_6H_4$(c)→$Ti_2O_6H_4^+$(c)	213.3	175.2	212.2	212.9	215.2
$Ti_2O_6H_4^+$(c)→$Ti_2O_6H_4^{2+}$(c)	318.0	191.5	315.6	318.4	316.6
$Ti_2O_6H_3^-$(c)→$Ti_2O_6H_3$(b)	81.0	133.6	72.4	80.5	79.8
$Ti_2O_6H_3^-$(a)→$Ti_2O_6H_3$(a)	105.6	152.0	102.4	105.4	105.4
$Ti_2O_6H_3$(a)→$Ti_2O_6H_3^+$(a)	209.1	169.2	209.0	210.6	213.2
$Ti_2O_6H_3$(b)→$Ti_2O_6H_3^+$(b)	199.9	158.5	202.0	200.0	199.8
$Ti_2O_6H_2^-$(a)→$Ti_2O_6H_2$(a)	93.1	136.0	84.1	93.9	94.3
$Ti_2O_6H_2^-$(b)→$Ti_2O_6H_2$(b)	97.1	138.2	96.6	98.0	98.5

Reactions	ΔE^{0K} B3LYP/ TZV(d,p) (kcal/mol)	ΔE^{0K} PCM-B3LYP/ TZV(d,p) (kcal/mol)	ΔE^{0K} CCSD/ TZV(d,p) (kcal/mol)	ΔH^{298K} B3LYP/ TZV(d,p) (kcal/mol)	ΔG^{298K} B3LYP/ TZV(d,p) (kcal/mol)
$Ti_2O_6H^-(a) \rightarrow Ti_2O_6H(a)$	124.2	174.3	112.9	126.1	127.3
$Ti_2O_6H^-(b) \rightarrow Ti_2O_6H(b)$	107.7	146.4	82.6	107.4	105.9
$Ti_2O_6^{2-} \rightarrow Ti_2O_6^-$	8.6	-213.2	-19.8	10.2	9.5
$Ti_2O_6^- \rightarrow Ti_2O_6$	53.1	94.8	57.2	53.9	54.1

Table 6

Reaction Energies in Gas Phase and Aqueous Phase for Proton Loss Reactions in Alkaline Medium

Reactions	ΔE^{0K} B3LYP/ TZV(d, p) (kcal/mol)	ΔE^{0K} PCM-B3LYP/ TZV(d, p) (kcal/mol)	ΔE^{0K} CCSD/ TZV(d, p) (kcal/mol)	ΔH^{298K} B3LYP/ TZV(d, p) (kcal/mol)	ΔG^{298K} B3LYP/ TZV(d, p) (kcal/mol)	□□□
$Ti_2O_5H_2(a)+OH^- \rightarrow Ti_2O_5H^-(a)+H_2O$	-72.2	-33.4	-74.8	-70.0	-61.0	-7.1
$Ti_2O_5H_2(b)+OH^- \rightarrow Ti_2O_5H^-(a)+H_2O$	-88.1	-45.7	-74.6	-86.1	-76.5	-16.3
$Ti_2O_5H_2(b)+OH^- \rightarrow Ti_2O_5H^-(b)+H_2O$	-87.7	-44.6	-74.9	-85.7	-76.1	15.5
$Ti_2O_5H_2^+(a)+OH^- \rightarrow Ti_2O_5H(a)+H_2O$	-190.0	-65.9	-194.0	-187.8	-178.6	30.9
$Ti_2O_5H_2^+(b)+OH^- \rightarrow Ti_2O_5H(a)+H_2O$	-200.6	-65.9	-198.3	-199.2	-190.3	-31.5
$Ti_2O_5H^-(a)+OH^- \rightarrow Ti_2O_5^{2-}+H_2O$	40.7	-3.5	40.9	41.8	50.1	14.0
$Ti_2O_5H(a)+OH^- \rightarrow Ti_2O_5^-+H_2O$	-80.6	-39.7	-82.3	-78.7	-69.6	-11.9
$Ti_2O_5H(b)+OH^- \rightarrow Ti_2O_5^-+H_2O$	-95.0	-49.9	-92.7	-92.7	-83.0	-19.1
$Ti_2O_6H_4(c)+OH^- \rightarrow Ti_2O_6H_3^-(b)+H_2O$	-77.1	-36.5	-79.8	-75.0	-64.6	-9.4
$Ti_2O_6H_4(c)+OH^- \rightarrow Ti_2O_6H_3^-(a)+H_2O$	-90.9	-48.7	-91.3	-90.6	-82.9	-19.7
$Ti_2O_6H_4(c)+OH^- \rightarrow Ti_2O_6H_3^-(c)+H_2O$	-54.0	-21.6	-52.8	-52.5	-43.9	0.9
$Ti_2O_6H_4^+(c)+OH^- \rightarrow Ti_2O_6H_3(a)+H_2O$	-198.6	-71.9	-201.1	-198.1	-192.6	-36.5
$Ti_2O_6H_4^+(c)+OH^- \rightarrow Ti_2O_6H_3(c)+H_2O$	-177.4	-56.4	-189.2	-174.7	-166.1	-23.6
$Ti_2O_6H_3(b)+OH^- \rightarrow Ti_2O_6H_2^-(a)+H_2O$	-96.4	-51.6	-86.1	-94.9	-85.5	-21.0
$Ti_2O_6H_3(b)+OH^- \rightarrow Ti_2O_6H_2^-(b)+H_2O$	-83.8	14.4	-86.1	-81.3	-71.5	28.1
$Ti_2O_6H_3(b)+OH^- \rightarrow Ti_2O_6H_2^-(c)+H_2O$	-92.7	7.6	-89.6	-91.6	-84.6	22.1
$Ti_2O_6H_3(a)+OH^- \rightarrow Ti_2O_6H_2^-(a)+H_2O$	-84.0	-43.0	-77.7	-81.6	-72.1	-14.0
$Ti_2O_6H_3(a)+OH^- \rightarrow Ti_2O_6H_2^-(b)+H_2O$	-72.3	-33.0	-78.7	-68.8	-58.9	-5.9
$Ti_2O_6H_3^+(b)+OH^- \rightarrow Ti_2O_6H_2(a)+H_2O$	-203.2	-74.2	-203.9	-201.0	-191.0	-36.9
$Ti_2O_6H_3^+(b)+OH^- \rightarrow Ti_2O_6H_2(b)+H_2O$	-187.5	-62.0	-192.6	-184.0	-173.7	-27.2
$Ti_2O_6H_2(a)+OH^- \rightarrow Ti_2O_6H^-(a)+H_2O$	-45.1	-12.6	-47.4	-43.1	-34.6	7.9
$Ti_2O_6H_2(a)+OH^- \rightarrow Ti_2O_6H^-(b)+H_2O$	-23.7	18.7	-12.0	-20.6	-10.5	31.7

Reactions	ΔE^{0K} B3LYP/ TZV(d, p) (kcal/mol)	ΔE^{0K} PCM-B3LYP/ TZV(d, p) (kcal/mol)	ΔE^{0K} CCSD/ TZV(d, p) (kcal/mol)	ΔH^{298K} B3LYP/ TZV(d, p) (kcal/mol)	ΔG^{298K} B3LYP/ TZV(d, p) (kcal/mol)	□□□
$Ti_2O_6H_2(b)+OH^- \rightarrow Ti_2O_6H^-(a)+H_2O$	-60.8	-24.7	-58.8	-60.1	-52.0	-1.8
$Ti_2O_6H_2(b)+OH^- \rightarrow Ti_2O_6H^-(b)+H_2O$	-39.4	6.6	-23.4	-37.5	-27.8	22.0
$Ti_2O_6H(a)+OH^- \rightarrow Ti_2O_6^-+H_2O$	-92.8	-46.7	-94.3	-92.5	-84.7	-18.3
$Ti_2O_6H(b)+OH^- \rightarrow Ti_2O_6^-+H_2O$	-97.7	-50.1	-99.3	-96.3	-87.5	-20.0

Coupled cluster calculations

Since coupled cluster calculations have been shown to improve the reaction energy for the $H_2O \rightarrow H_2 + ½ O_2$ reaction, single point CCSD energies for optimized structures of $Ti_2O_5H_2$ and $Ti_2O_6H_4$ derivatives are calculated. Tables 4, 5, and 6 list coupled cluster reaction energies, which are comparable with B3LYP energies. In proton loss steps of the one water molecule addition case, reaction energies are ~3-20 kcal (up to 6%) higher than B3LYP energies in gas phase (Table 4) and differ by -4 to +15 kcal/mol in alkaline medium (Table 6). Similarly, electron loss energies in the one water molecule case are generally lower by ~1-9 kcal/mol (Table 5).

CCSD reaction energies for two water molecules with Ti_2O_4 are also comparable with calculated B3LYP energies. As calculated in the one water case, CCSD gas phase proton loss energies are higher by 4-20 kcal/mol and the energies are lower by +16 to -5 kcal/mol in alkaline medium. These CCSD calculations suggest that the results obtained at the B3LYP/TZV(d, p) level of theory are fairly reasonable.

Overall reaction profiles

The overall reaction profiles for water splitting on Ti_2O_4 are shown in Figure 7 at both the B3LYP and PCM-B3LYP levels of theory. As calculated in section 3.1, the reaction energy for $2H_2O \rightarrow 4H^+ + 4e^- + O_2$ at the B3LYP/TZV(d, p) level of theory is calculated to be 1588.12 kcal/mol (1188.04 kcal/mol with PCM-B3LYP). Since the water splitting process represents a thermodynamic cycle, the overall reaction energy found in this work is also 1588.12 (1188.04) kcal/mol. Because of exothermic water addition and because of catalyst rearrangement, the endothermicity of the proton and electron removal steps is higher at 1795.36 (1342.8) kcal/mol. We expect that a larger cluster will have lower water adsorption energies and that catalyst rearrangement will not be as significant, which will reduce the additional endothermicity induced by these processes. In addition, the O_2 removal step would not be as endothermic.

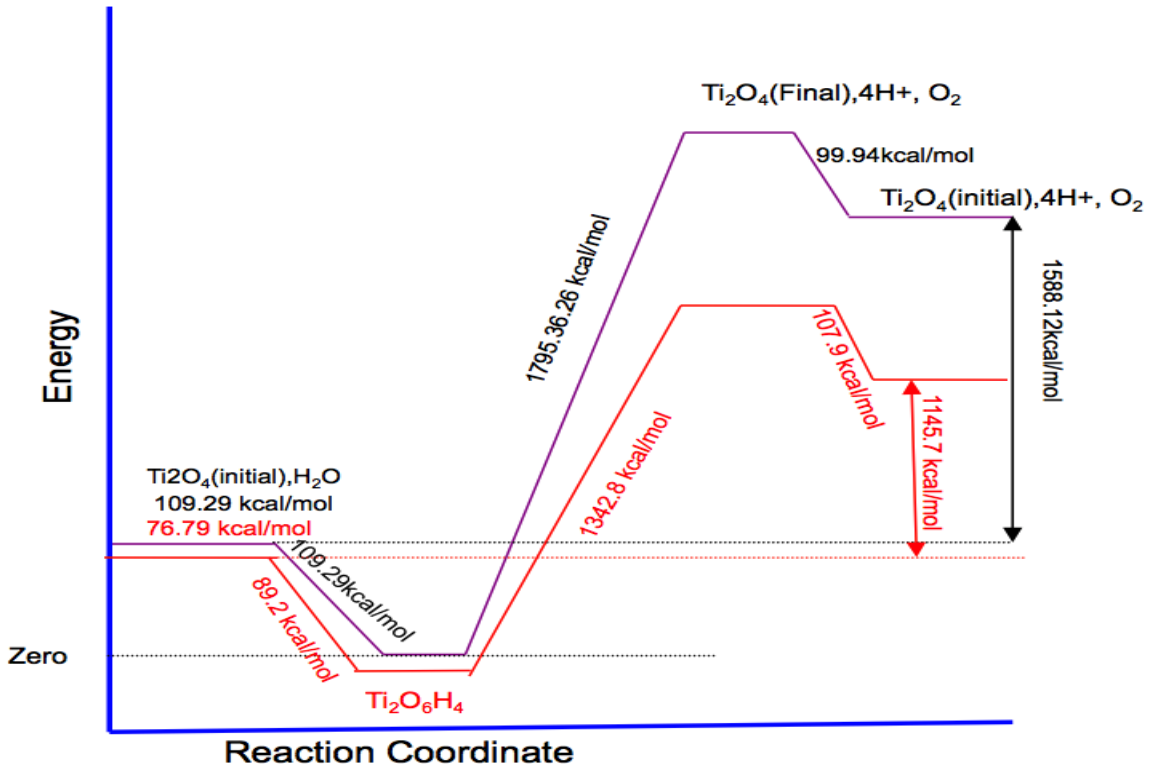

Figure 7: *Overall Reaction Profile. Purple: Gas Phase; Red: Aqueous Phase.*

Reaction energies under applied voltage

Under electrochemical conditions, a voltage is applied to the cell that affects reaction energies. Reaction steps for hydrogen loss with respect to standard hydrogen electrode (SHE) have been drawn in Figure 7; only gas phase reaction energies are considered in this figure. The SHE potential (i.e. the free energy of the $H^+ + e^- \rightarrow ½\ H_2$ half-reaction) at the B3LYP/TZV(d, p) level is calculated to be 15.84 eV at 298 K. All the steps are found to be uphill at zero external potential with a wider gap in the third hydrogen release. Applying 1.23 eV (the minimum potential for water splitting), the fourth hydrogen loss would be a downhill process, but the first three steps would be uphill. The lowest energy structure of $Ti_2O_6H_3$ requires 2.14 eV (0.91 eV higher than the minimum potential required for water splitting). In addition, at 2.14 eV, the second hydrogen and fourth hydrogen losses would be favorable. As calculated the energy of most stable structure of Ti_2O_6H is 9.2 eV; an external potential of 3.2 V makes the process almost down hill. An external potential of 3.4 eV makes the reaction completely downhill other than the step in which O_2 is released.

With the application of an external potential, new pathways become possible. For example, several $Ti_2O_6H_2$ species are lower in energy than $Ti_2O_6H_3$ species when an external potential of 3.1 eV is applied. Thus, the reaction could proceed in several ways. Since triplet states are higher in energy than singlet states for the titanium-containing intermediates, it is possible that a pathway may lead to e.g. triplet Ti_2O_6, which could then dissociate in a straightforward manner to triplet O_2 and singlet Ti_2O_4. Further work needs to be done in this area.

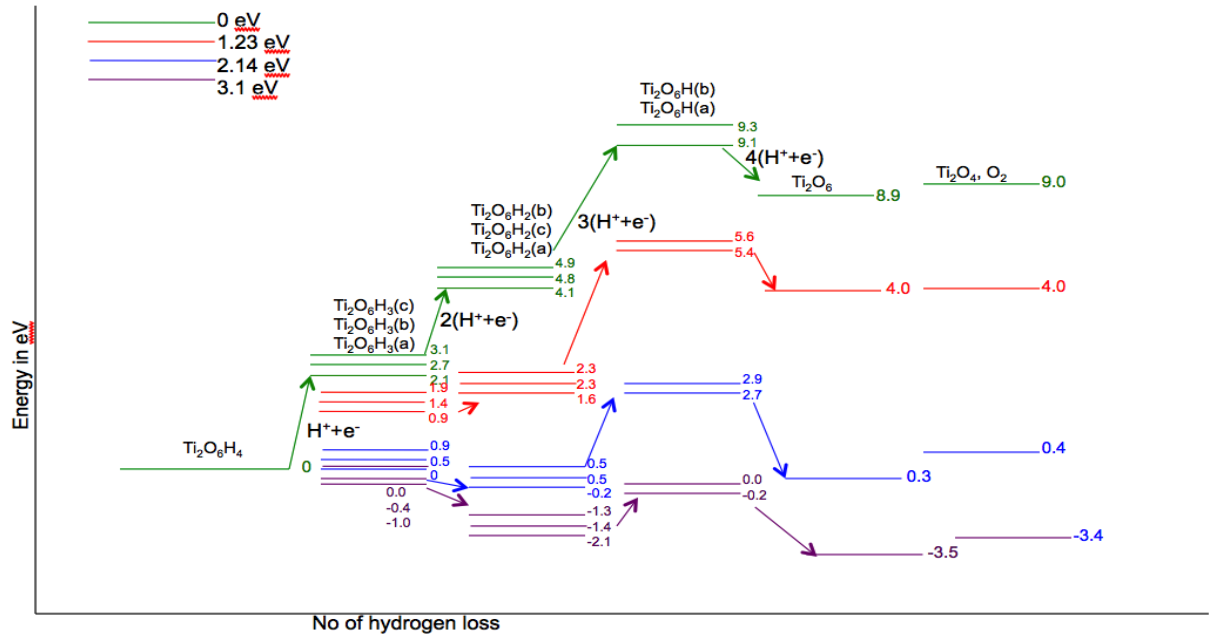

Figure 8: Reaction Energies (eV) of Hydrogen Loss Species of $Ti_2O_6H_4$ with Respect to Standard Hydrogen Electrode.

Conclusion

Water splitting has been examined in a step-by-step manner on a Ti_2O_4 model catalyst. Water adsorbs exothermically on this cluster and is predicted to spontaneously transfer one proton to a bridging or terminal oxygen atom. Individual proton and electron removal steps have been investigated for both one and two water molecules and are found to be highly endothermic both in the gas phase and in a continuum aqueous phase. However, in alkaline media the proton removal steps are predicted to be favorable. Coupled cluster single point energies are in good agreement with the B3LYP values calculated in this work.

O-O bonds form after only two electrons are removed from the system, which suggests that these bonds form early in the water splitting process. For a single water molecule, removal of a single electron is sufficient to lead to O-O bond formation. These bonds have a single bond character that is characteristic of peroxides. However, in contrast to several previous studies, HOO-containing species are found to be high-energy intermediates in this work, which suggests that future investigations could also consider pathways that do not go through peroxides.

Reaction energies under applied voltage are also calculated with respect to SHE. A voltage of 3.1 eV is required to make the reaction downhill. This voltage is larger than the one calculated in previous work, which is likely due to the use of a cluster model in the current work; the water adsorption and catalyst rearrangement energies contribute to a higher overpotential.

References

Anpo, M., Dohshi, S., Kitano, M., & Hu, Y. (2006). Metal oxides: Chemistry and applications (J. L. G. Fierro, Ed.). CRC Press.

Asahi, R., Morikawa, T., Ohwaki, T., Aoki, K., & Taga, Y. (2001). Visible-light photocatalysis in nitrogen-doped titanium oxides. Science, 293(5528), 269–271. https://doi.org/10.1126/science.1061057

Bandyopadhyay, I., & Aikens, C. M. (2011). Structure and bonding of $Ti_nO_{2n}^{+1}$ clusters. Journal of Physical Chemistry A, 115(5), 868–879. https://doi.org/10.1021/jp109944m

Brinkley, T., Dietrich, M., Engel, T., Farrall, P., Gantner, G., Schäfer, A., & Szuchmacher, A. (1998). The structure and chemistry of the Cu(100)–O surface: From adsorbed atomic oxygen to the "added row" phase. Surface Science, 395(2–3), 292–302. https://doi.org/10.1016/S0039-6028(97)00707-3

Calatayud, M., Maldonado, L., & Minot, C. (2008). Adsorption of small aromatic N-heterocyclic molecules on anatase (101) TiO_2. Journal of Physical Chemistry C, 112(42), 16087–16095. https://doi.org/10.1021/jp804678w

Di Valentin, C., Pacchioni, G., Selloni, A., Livraghi, S., & Giamello, E. (2005). Characterization of paramagnetic species in N-doped TiO_2 powders by EPR spectroscopy and theoretical calculations. Journal of Physical Chemistry B, 109(23), 11414–11419. https://doi.org/10.1021/jp051587q

Fujishima, A., & Honda, K. (1972). Electrochemical photolysis of water at a semiconductor electrode. Nature, 238(5358), 37–38. https://doi.org/10.1038/238037a0

Hagfeldt, A., Bergström, R., Siegbahn, H. O. G., & Lunell, S. (1993). Electron localization in dye-sensitized nanocrystalline TiO_2—an experimental and theoretical study. Journal of Physical Chemistry, 97(50), 12725–12730. https://doi.org/10.1021/j100153a021

Henderson, M. A. (1998). The interaction of water with solid surfaces: Fundamental aspects revisited. Surface Science, 395(2–3), 151–170. https://doi.org/10.1016/S0039-6028(97)00638-4

Hugenschmidt, M. B., Gamble, L., & Campbell, C. T. (1994). The interaction of H_2O with a TiO_2(001) surface. Surface Science, 302(1–2), 329–337. https://doi.org/10.1016/0039-6028(94)90714-5

Hussain, A., Gracia, J., Nieuwenhuys, B. E., & Niemantsverdriet, J. W. (2010). Reactive oxygen on reducible oxides: The role of lattice oxygen in Pd-catalyzed CO oxidation. ChemPhysChem, 11(11), 2375–2382. https://doi.org/10.1002/cphc.201000225

Hyman, M. P., & Medlin, J. W. (2005). Density functional theory analysis of NO adsorption on rutile-supported vanadium oxide catalysts. Journal of Physical Chemistry B, 109(13), 6304–6310. https://doi.org/10.1021/jp045525h

Hyman, M. P., & Medlin, J. W. (2006). Reaction pathways for NO reduction by hydrogen on rutile-supported vanadium oxide catalysts. Journal of Physical Chemistry B, 110(32), 15338–15344. https://doi.org/10.1021/jp062440g

Jeong, K. S., Chang, C., Sedlmayr, E., & Sülze, D. (2000). Electronic structure of small titanium oxide clusters. Journal of Physics B: Atomic, Molecular and Optical Physics, 33(16), 3417–3430. https://doi.org/10.1088/0953-4075/33/16/312

Karvinen, S., Hirva, P., & Pakkanen, T. A. (2003). Computational study of the adsorption of NO_2 on the TiO_2(110) surface. Journal of Molecular Structure: THEOCHEM, 626(1–3), 271–277. https://doi.org/10.1016/S0166-1280(03)00260-4

Li, S., & Dixon, D. A. (2008). The structure and bonding of TiO_2 nanoclusters. Journal of Physical Chemistry A, 112(28), 6646–6666. https://doi.org/10.1021/jp801768t

Li, Y.-F., Liu, Z.-P., Liu, L., & Gao, W. (2010). Mechanism for TiO_2 anatase/rutile phase transformation: Reaction coordinate and electronic structure. Journal of the American Chemical Society, 132(35), 13008–13015. https://doi.org/10.1021/ja104721h

Lindan, P. J. D., & Zhang, C. (2005). Exciton-trapping sites in porous silica. Physical Review B, 72(7), Article 075439. https://doi.org/10.1103/PhysRevB.72.075439

Meng, Q.-Q., Wang, J.-G., Xie, Q., Dong, H.-Q., & Li, X.-N. (2011). Hydrothermal synthesis of TiO_2 nanowires for photocatalysis. Catalysis Today, 165(1), 145–149. https://doi.org/10.1016/j.cattod.2010.11.049

Nakamura, R., & Nakato, Y. (2004). Role of oxygen vacancy in the plasma-treated TiO_2 photocatalyst with visible light sensitivity. Journal of the American Chemical Society, 126(4), 1290–1298. https://doi.org/10.1021/ja037172k

Nakamura, R., Okamura, T., Ohashi, N., Imanishi, A., & Nakato, Y. (2005). Shift of the flatband potential of rutile TiO_2 to the positive side by ultraviolet irradiation and its photocatalytic activity. Journal of the American Chemical Society, 127(44), 12975–12983. https://doi.org/10.1021/ja053481b

Pliego, J. R., Jr., & Riveros, J. M. (2001). The cluster-continuum model for the calculation of the solvation free energy of small molecules. Journal of Physical Chemistry A, 105(30), 7241–7247. https://doi.org/10.1021/jp010509f

Pliego, J. R., Jr., & Riveros, J. M. (2002). The cluster-continuum model for solvation effects: The case of the SN2 reaction of fluoride ion with methyl chloride. Journal of Physical Chemistry A, 106(35), 7434–7439. https://doi.org/10.1021/jp020284g

Qu, Z.-W., & Kroes, G.-J. (2006). Theoretical investigation of water dissociation on rutile TiO_2(110). Journal of Physical Chemistry B, 110(19), 8998–9007. https://doi.org/10.1021/jp057476v

Rossmeisl, J., Qu, Z.-W., Zhu, H., Kroes, G.-J., & Nørskov, J. K. (2007). Electrolysis of water on oxide surfaces. Journal of Electroanalytical Chemistry, 607(1–2), 83–89. https://doi.org/10.1016/j.jelechem.2007.01.008

Schmidt, M. W., Baldridge, K. K., Boatz, J. A., Elbert, S. T., Gordon, M. S., Jensen, J. H., Koseki, S., Matsunaga, N., Nguyen, K. A., Su, S., Windus, T. L., Dupuis, M., & Montgomery, J. A., Jr. (1993). General atomic and molecular electronic structure system. Journal of Computational Chemistry, 14(11), 1347–1363. https://doi.org/10.1002/jcc.540141112

Shankar, K., Tep, K. H., Mor, G. K., & Grimes, C. A. (2006). Photoinduced charge transfer in anodized TiO_2 nanotubes. Journal of Physics D: Applied Physics, 39(11), 2368–2375.

Túnon, I., Silla, E., & Tomasi, J. (1992). Microsolvation effects on the proton transfer between ammonia and hydrogen chloride. Journal of Physical Chemistry, 96(23), 9043–9048. https://doi.org/10.1021/j100200a006

Valdés, Á., & Kroes, G.-J. (2010). Molecular dynamics study of the oxygen evolution reaction on rutile TiO_2(110). Journal of Physical Chemistry C, 114(4), 1701–1708. https://doi.org/10.1021/jp909460g

Valdés, Á., Qu, Z.-W., Kroes, G.-J., Rossmeisl, J., & Nørskov, J. K. (2008). Oxidation and reduction of water on the oxygen-terminated and hydrogen-terminated (0001) surfaces of rutile α-quartz. Journal of Physical Chemistry C, 112(26), 9872–9879. https://doi.org/10.1021/jp802151w

Wang, T.-H., Fang, Z., Gist, N. W., Li, S., Dixon, D. A., & Gole, J. L. (2011). Water adsorption on oxidized single crystal and nanoporous SnO_2 from classical molecular dynamics simulations. Journal of Physical Chemistry C, 115(20), 9344–9360. https://doi.org/10.1021/jp111932k

Xu, J. P., Wang, J. F., Lin, Y. B., Liu, X. C., Lu, Z. L., Lu, Z. H., Lv, L. Y., & Du, Y. W. (2007). Large magnetocaloric effect in $La_{0.7}Ca_{0.3}MnO_3$ nanotube arrays with hollow interior. Journal of Physics D: Applied Physics, 40(10), 3005–3009.

Zhai, H.-J., & Wang, L.-S. (2007). Probing the electronic structure of neutral and anionic TiO_2 clusters. Journal of the American Chemical Society, 129(10), 3022–3027. https://doi.org/10.1021/ja067698z